Electronic Supplementary Material (ESI) for Reaction Chemistry & Engineering.

One line in the two uses: TiO_x-C displays either photocatalyst or thermocatalyst to motivate reductive amination

Shun Wang,[a] Xinli Tong, [a,] * Lingwu Meng, [a] Yujun Zhao[b]

[a] *Tianjin Key Laboratory of Organic Solar Cells and Photochemical Conversion, School of Chemistry and Chemical Engineering, Tianjin University of Technology, No. 391 Binshuixi Road, Tianjin 300384, P. R. China. Tel: (+86)-22-60214259; E-mail: tongxinli@tju.edu.cn; tongxli@sohu.com.*

[b] *School of Chemical Engineering and Technology, Tianjin University, Tianjin 300072, P. R. China.*

Supporting Information

1. The XRD patterns of catalysts

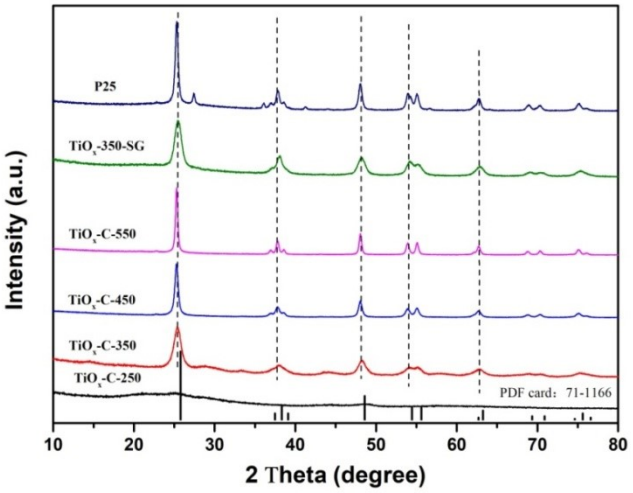

Figure S1. XRD patterns of different titanium oxide samples

The X-ray diffraction patterns of different titanium oxide-based materials were shown in Figure S1. After the calcination treatment, several typical oxide peaks could be obviously formed except for the TiO_x-C-250 sample. Moreover, the major characteristic peaks of these catalytic materials including TiO_x-C-350, TiO_x-C-450, TiO_x-C-550, TiO_x-350-SG and P25 were at 2θ of 25.3, 37.8, 48.0, 53.0 55.7 and 62.1°, which is consistent with the typical anatase phase (JCPDS No. 71-1166). Further observations revealed that characteristic peaks of TiO_x-C-350 have been broadened

compared to the TiO_x-C-450, TiO_x-C-550 and P25 materials, which indicates that doping of carbon element arises the crystal size to decrease. On the other hand, the average particle size of TiO_x-C-350, TiO_x-C-450, and TiO_x-C-550 were 75 nm, 169 nm and 271 nm respectively by using the Scherrer's equation. Obviously, the temperature increase will cause particle aggregation and the decrease of the specific surface area. …

2. The SEM images of catalysts

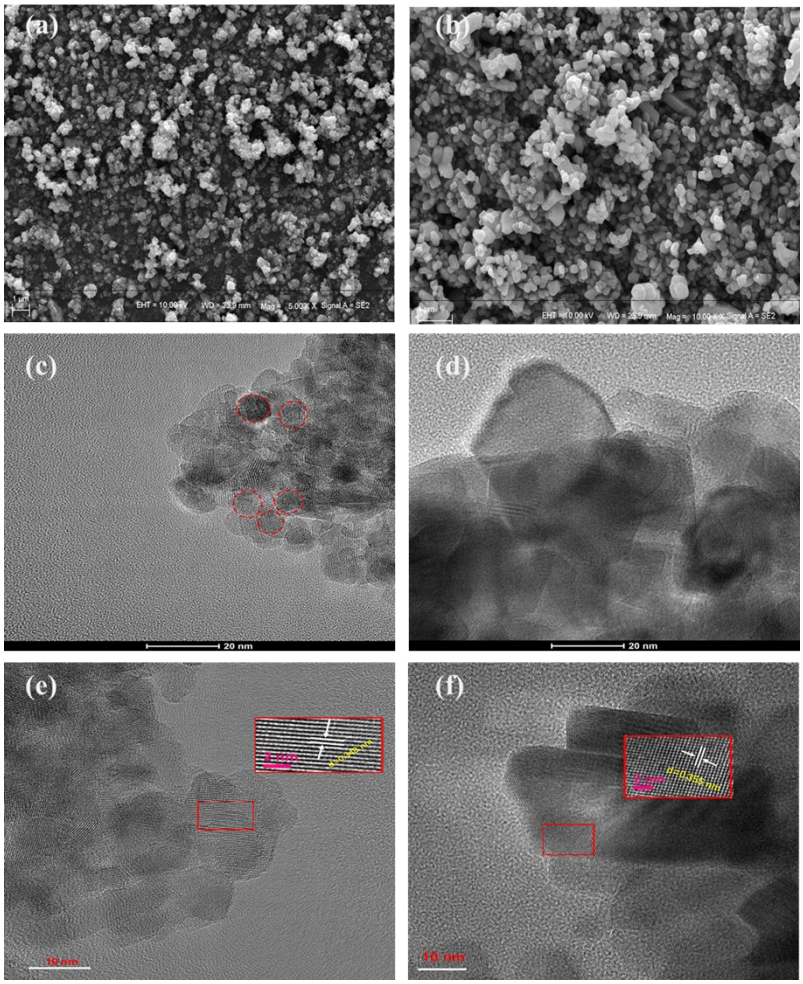

Figure S2. The SEM images of TiO_x-C-350 (a) and TiO_x-C-550 (b) and the HRTEM of TiO_x-C-350 (c,e) and TiO_x-C-350 (d, f) materials

On Figure S2, the FESEM images revealed the morphologies of the TiO_x-C-350 and TiO_x-C-550 catalysts. As shown in Figures S2a and S2b, TiO_x-C-350 and TiO_x-C-550 are composed of spherical particles, in which the size of TiO_x-C-550 was larger than that of TiO_x-C-350 material. Therefore, the high-temperature treatment could lead to agglomeration of particles and loss of C component in the catalyst. Seen from

the HRTEM results, TiO_x-C-350 was constituted of spherical particles approximately 6-12 nm in diameter with relative distinct boundaries. However, there was no occurrence of relative boundary on TiO_x-C-550 catalyst (Figures S2c and S2d). Therefore, it is concluded that the shell structure of TiO_x-C-350 was due to the accumulation of the TiO_x interstitial C component. By Digital Micrograph (DM) software, it is found that the lattice spacing of TiO_x-C-350 and TiO_x-C-550 kept at d = 0.348 nm and 0.355 nm, respectively, which were ascribed to the (1 0 1) plane of anatase titanium oxide (Figures S2e and S2f). Thus, the TiO_x-C-350 catalyst surface should include the structure of Ti-O-C which can affect the lattice spacing of titanium oxide.

3. The TEM images of catalysts

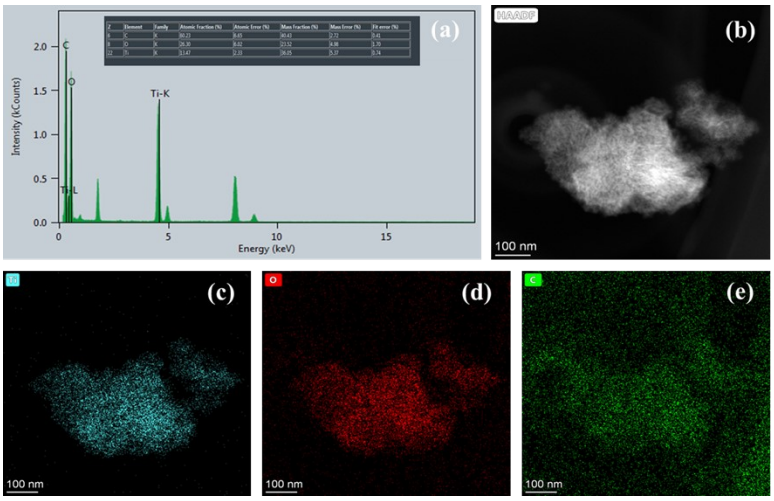

Figure S3. (a) The EDX spectra of TiO_x-C-350; (b) The HRTEM images of selected area of TiO_x-C-350, and the corresponding EDX mapping images for (c) Ti element, (d) O element and (e) C element

The composition and distribution of elements in TiO_x-C-350 catalyst were investigated by the energy dispersive X-ray (EDX) and HRTEM elemental mapping, and the results are presented on the Figure S3. Therein, the element composition of the sample are determined according to the characteristic X-ray wavelengths of different elements, and the atomic fraction of O, Ti and C was 26.30 %, 13.47 % and 60.23 %, respectively. In particular, the atomic ratio of O and Ti is about 1.95, which showed that the stuucture of Ti-O-C was formed. It should be noted that the amount of C element of TiO_x-C-350 material was affected by the ultra-thin carbon support

film so that it is more than those of Ti and O element. Furthermore, it is found that the homogeneous distribution of Ti, O and C across the entire selected area was achieved.

4. The FT-IR characterization of catalysts

The IR and Roman spectra of different catalysts are provided in Figure S4. It is found that the broad peaks at about 3411 cm^{-1} and 1639 cm^{-1} should belong to the vibration of -OH and the bending vibration of water which adsorbed on the surface of the catalyst. The peaks at 2938 cm^{-1} and 2871 cm^{-1} could be contributed to the $-CH_2$ vibration during the process of the catalyst preparation (Figure S4a). Further, by the partial enlargement of IR spectrum, the peaks at 1082 cm^{-1} and 1040 cm^{-1} were related to C-O bond stretching vibration. Moreover, it was seen that the peaks of 1040 cm^{-1} and 886 cm^{-1} disappear along with the proceeding of catalyst preparation. However, a new peak appear at 922 cm^{-1} for the precursor and catalyst. Meanwhile, it is found that, from the results of photocatalyst TiO_x-C at different calcination temperatures, the peak of 922 cm^{-1} only exists at 350 °C and 250 °C (shown in the Figure S4c). Therefore, it can be concluded that the C-O bond at the 1040 cm^{-1} disappear slowly and the Ti-O bond was formed when the $TiCl_4$ was added in the EG. Also, the C-C bond have been changed (the peak at 886 cm^{-1}) owning to the formation of the Ti-O bond. As the calcination temperature increases, the C-C bond broken and the C-H bond disappear at the bigining. When it was treated at 350 °C, not only the characteristic peak (during 500-700 cm^{-1}) of titanium oxide appeared obviously but also the new peak at 922 cm^{-1} appeared. Therefore, in the case of the catalyst,the structure of O-Ti-O and C-O-Ti existed simultaneously at the 350 °C. The peak at 922 cm^{-1} probably belong to the C-O bond of C-O-Ti structure. When the calcination temperature beyond 350 °C, the C-O bond of the C-O-Ti structure would be broken, leading that the peak of 922 cm^{-1} also disappeared and only the O-Ti-O structures at the range of 400-1500 cm^{-1} were left.

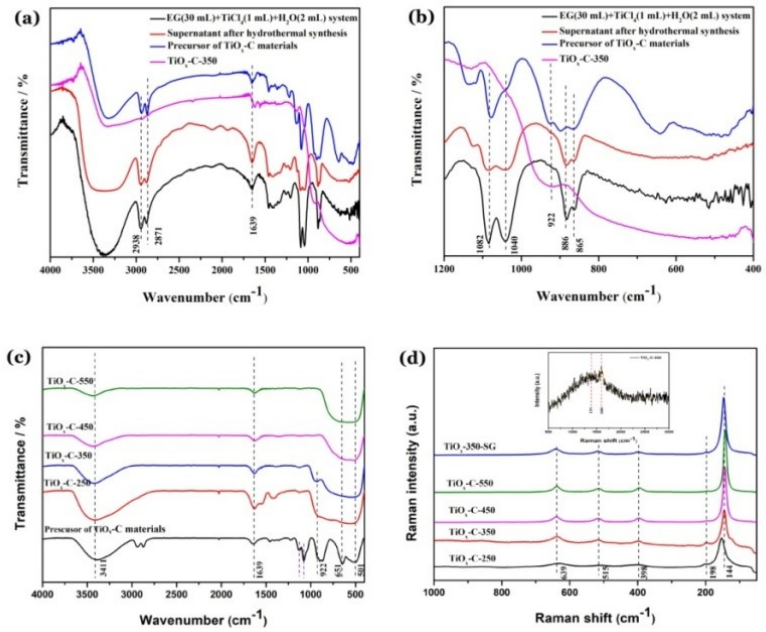

Figure S4. (a) The FT-IR spectra for the process of the TiO_x-C -350 preparation; (b) Partial enlargement of picture (a) at the range of 400-1200 cm^{-1} wavenumber; (c) FT-IR spectra of TiO_x-C materials at different calcination temperature; (d) The Raman spectra of different TiO_x-C samples

5. The Roman detection of catalysts

In the Raman spectra, these as-prepared TiO_x-C catalytic materials and TiO_x-350-SG sample possessed the characteristic peaks at 144, 198, 398, 515 and 639 cm^{-1}, respectively, so the corresponding skeleton of the crystallines belonged to the antaste form of titanium oxide. The E_g peak included the characteristic ones at 144, 198 and 639 cm^{-1}, which could be caused by the symmetric stretching vibration of O-Ti-O form, and are mainly attributed to Ti-O band of (1 0 1) surface of TiO_x-C material. In addtion, the A_{1g} peak (515 cm^{-1}) and B_{1g} peak (398 cm^{-1}) can be caused by the asymmetric bending vibration and symmetric bending vibration of O -Ti- O, and are attributed to the Ti-O bond on the (0 0 1) surface of the TiO_x-C catalyst. Moreover, seen from the Figure S4d, the characteristic peak intensity at 144 cm^{-1} increased with the increase of the calcined temperature, while the characteristic peak intensity at 198 cm^{-1} became weaker. Among them, the characteristic peaks of TiO_x-C-350 catalyst at 144 cm^{-1} and 198 cm^{-1} were relatively obvious, indicating that the stretching vibration of O-Ti-O was affected at this time. Combined with the partial enlarged view of the

Raman spectrum of TiO_x-C-350, there were two small peaks at 1391 and 1604 cm^{-1}, which should be caused by the disordered C element. Therefore, it is inferred that the TiO_x-C-350 catalyst owns the C-O-Ti structure.

6. The XPS spectrum of catalyst

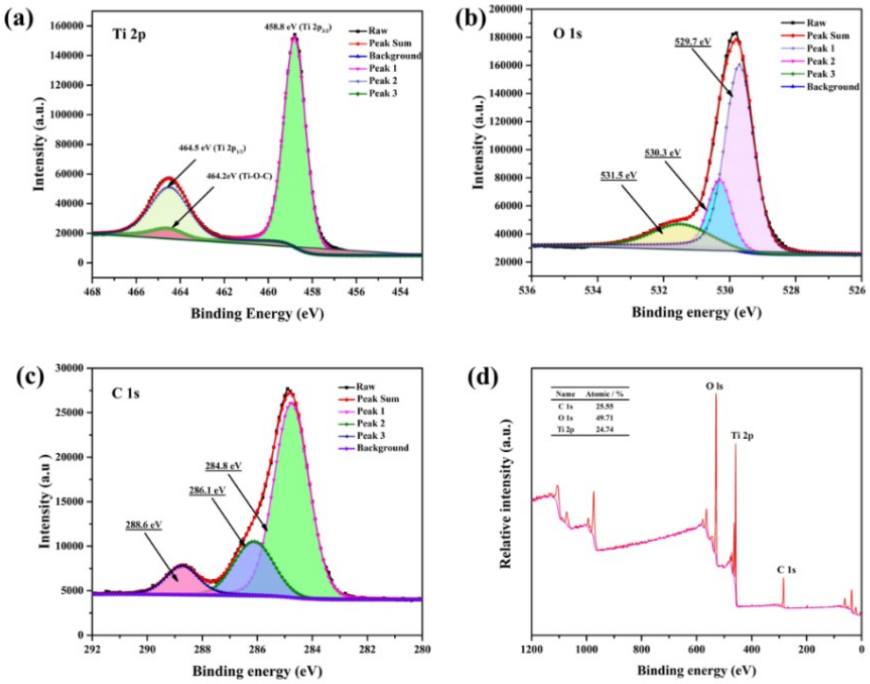

Figure S5. (a) Ti 2p, (b) C 1s and (c) O 1s X-ray photoelectron spectra of TiO_x-C-350. (d) XPS profiles of full scan

The XPS spectra of TiO_x-C-350 were shown in the Figure S5. The two peaks at 458.8 and 464.5 eV were ascribed to the Ti $2p_{3/2}$ and Ti $2p_{1/2}$ signals, respectively, and no any peak at about 457.0 eV was found, which might be assigned to Ti^{3+} signal. Moreover, there existed an another relatively weak peak located at 464.2 eV on the Ti 2p spectrum, which was ascribed to the Ti-O-C bond. As for the Ti-O-C sample, the peaks of Ti 2p component exerted a slight red shift of 0.4 eV / 0.2 eV compared with those of precursor/TiO_x-C-550, the higher binding energy values of Ti 2p in TiO_x-C-350 indicated the higher positive charge on Ti atoms of the TiO_x-C-350 than that of the precursor and TiO_x-C-550 material, which may be due to the carbon coating. Also, the O 1s signals were multicomponent, with the most intense peak at 529.7 eV due to lattice oxygen in titanium oxide, and the less intense peak 530.3 eV was ascribed to

the oxygen of C-O-Ti, and the peak at 531.5 eV was attributed to defective oxygen. The C 1s spectrum showed the most intensity peak at 284.8 eV. To access the surface carbon species, the curve fitting of C 1s signals had been also performed, the dominant peak at 284.8 eV was due to the existence of the disordered carbon that is consistent with the peaks of 1391 and 1604 cm^{-1} in Raman spectrum of the TiO_x-C-350 catalyst. From the XPS of full scan (Figure 5d), the percentages of C, O and Ti were 25.55 %, 49.71 % and 24.74 % respectively. The peak at 286.1 eV could be assignable to the carbon of C-O-Ti coordination and the peak at 288.6 eV could be assigned to C=O group.

7. The BET data of catalysts

The results of BET detection are summarized in the Table S1. Along with the increase of calcination temperature, the specific surface area and pore volume of the material are gradually decreased, and the average pore size is slowly increased. Moreover, it is seen that the specific surface area was basically reduced by half for every increase of 100 °C of the calcination temperature, which is attributed to accumulation of nanoparticles at a relatively high temperature. Therein, the BET surface area and pore volume of TiO_x-C-350 kept at 122.2 m^2/g and 0.25 cm^3/g respectively, which is larger than those of the TiO_x-350-SG and P25 catalysts. The larger specific surface area and pore volume of TiO_x-C-350 catalyst facilitate the adsorption of the substrate on the surface.

Table S1. Textural properties of different titanium oxide-based catalysts

Catalyst	BET Surface Area (m^2/g)	Pore Volume (cm^3/g)	Average pore diameter (Å)	
			BJH adsorption	BJH desorption
TiO_x-C-250	218.9	0.24	35.95	35.31
TiO_x-C-350	122.2	0.25	50.77	49.55
TiO_x-C-450	66.6	0.16	59.08	59.23
TiO_x-C-550	31.4	0.11	61.38	71.83
TiO_x-350-SG	111.6	0.16	46.64	40.97
P25	50.6	0.16	48.26	51.44

8. TG curve

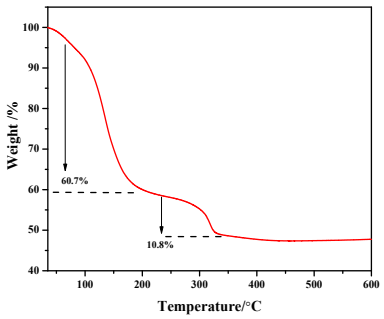

Figure S6. TG curve of catalyst precursor for preparation of TiO_x-C-350

9. The reaction mechanism of photocatalytic reductive amination of 3-phenylpropanal

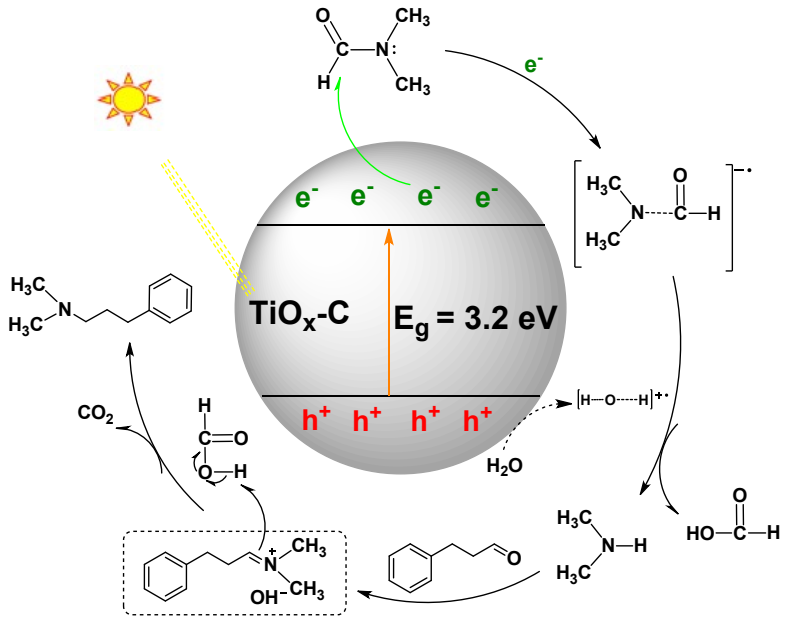

Figure S7. Proposed mechanism for the reductive amination of **1** with TiO_x-C-350 photocatalyst.

Based on above obtained reaction results and the typical photocatalysis theory, a mechanism for photocatalytic reductive amination of 3-phenyl propanal was proposed and presented in the Figure S7. Therein, the catalytic reductive amination of aldehyde with DMF was consisted of two steps: a) DMF and H_2O were decomposed into dimethylamine and formic by TiO_x-C-350 under light irradiation, where the electrons could be responsible for the activation of C-N bond in DMF molecule that impels the formation of dimethylamine and formaic acid. (b) the molecular aldehyde was firstly reacted with dimethylamine to form iminium ion via the condensation reaction and one water molecule is released, which was subsequently reduced by the *in situ* generated formic acid to generate the corresponding amine as the product.

10. The characterization of used catalyst

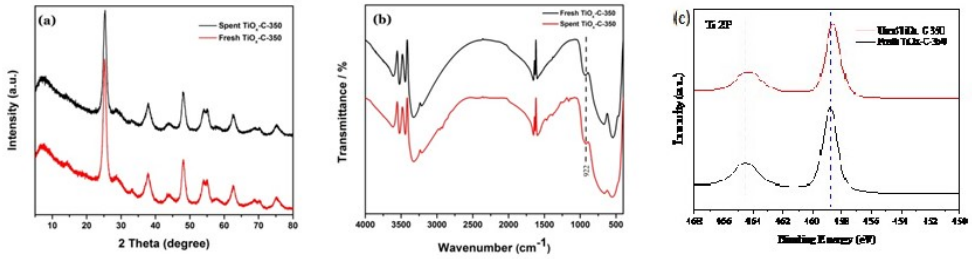

Figure S8. The XRD patterns (a), IR spectra (b) and XPS detection (c) of used and fresh catalysts

The XRD pattern and IR spectrum of the used catalyst are provided in the Figure S8 of the revised supporting information. Seen from the XRD results, the main feature peaks almost kept unchanged. However, the crystallinity was decreased a little. According to the IR results, several new peaks between 2600- 2800 cm^{-1} occurred in the used catalyst, which is possibly attributed to the absorption of the residue on the TiO_x-C catalyst surface. Based on the XPS data, it is concluded that the binding energy of used TiO_x-C was decreased. Therefore, it is concluded that the gradual decreasing of conversion could be due to the lower crystallinity and binding energy or less absorption sites of the used solid catalyst.

11. The comparison with the other catalytic systems

The comparison with the other systems was summarized in the following Table S2. It can be seen that the reductive amination with the this method is more promising due to the reaction conditions being milder in the presence of TiO_x-C solid catalyst.

Table S2. The comparison with the results of other catalytic systems

entry	Catalytic system	Temperature (°C)	References
1	typical Leuckart reaction	>180	*Ber. Dtsch. Chem. Ges.*, **1885**, 18, 2341-2344; *Tetrahedron Lett.*, **2013**, 54, 1835-1838
2	$Zn(OAc)_2$	150	*Adv. Synth. Catal.*, **2018**, 360, 485-490
3	ZrO_2	>140	Catal. Sci. Technol., 2018, 8, 5396–5400; *Mol. Catal.*, **2020**, 494, 111108
4	TiO_x-C	90; r. t. (light)	present work